International Journal of Recent Technology and Engineering (IJRTE)
ISSN: 2277-3878, Volume-8 Issue-3, September 2019

Research on Magnetic-Valve Controllable Reactor Based on ANSYS

Samuel Addo Darko, Mingxing Tian, Huiying Zhang

Abstract*: Magnetic-valve controllable reactor (MCR) has become many researcher's topic of the day because of its versatile use in power systems. MCR utilizes the concept of magnetic saturation to control power flows in the power grid. It is as simple to operate and maintain, and reliable as an ordinary transformer. However, magnetic-valve controllable reactor works under a more variety of complex excitation condition because of the superposition action of AC and DC excitations. This paper carefully discusses the distribution of magnetic field of MCR core, provides an understanding of the range of inductance adjustments and further analyzes the working current waveform. Based on that, the finite element analysis software ANSYS Maxwell is used to design and examine a 3-D prototype model under different control voltage levels. The method of transient solution is applied for the reason being that it simultaneously has both AC and DC voltages. The AC voltage is kept constant while the DC voltage is varied from the minimum to the maximum rated value. The simulation results confirm that the magnetic-valve controllable reactor works in the saturation region of the magnetization curve under the combined excitation of AC and DC. The inductance adjustment range shows that the MCR inductance value can be smoothly and continuously varied. In addition, the working output current contains little odd-order harmonics that can be mitigated if filtering device is used or the magnetic valves are designed carefully. By observing the simulation results and analysis, one can gain a thorough understanding of MCR under actual working condition. It provides a reliable basis for the performance design of magnetic-valve controllable reactor.

***Index Terms*: Magnetic-valve Controllable Reactor (MCR); Magnetic Field Distribution; Magnetic Saturation; Inductance Adjustment.**

I. INTRODUCTION

Nowadays, magnetic-valve controllable reactor (MCR) is of a great use in long distance high and extra high voltage transmission lines, and substations with high voltage fluctuation. It is also highly recommended for large-scale factories that need their own regulated source of reactive power. In practical application, MCR reduces grid losses, improves power quality, optimizes power transmission, control operations automatically, increases reliability and simplifies maintenance [1-7]. The research and application of MCRs have been greatly developed thereby, leading to many different types [8-10]. Many articles focus on MCR power losses, and some others also study into vibration and harmonic optimization. It is generally known that MCR works under a more variety of complex excitation conditions since the core has both AC and DC excitation conditions, and it is therefore, of great significance to study the specific characteristics of MCR under actual working conditions.

This paper mainly discusses the distribution of magnetic field of a core of MCR, the range of inductance adjustments and output waveform of working current, respectively. Finally, a simulation model is built with the use of ANSYS Maxwell Electromagnetic software to achieve excellent correlation to the practicality of MCR.

II. THE STRUCTURE AND WORKING PRINCIPLE

The core structure and winding arrangement of a single phase MCR are shown in Fig.1(a) and Fig.1(b), respectively. These consist of an iron core with magnetic valves, AC windings and DC windings. The AC windings are referred to as working windings and DC windings are referred to as control windings. The iron core has two parallel limbs and two side yokes. Working windings and control windings are fixed onto two limbs of the core. The equivalent circuit and simulation circuit of the single phase magnetic-valve controllable reactor are shown in Fig.2(a) and Fig.2(b), respectively. Where N_A is the number of working winding turns, N_D is the number of control windings turns, R_A is working winding resistance and R_D is control winding resistance. Terminals of the working windings are directly connected in parallel to the power grid. Terminals of the control windings are reversely connected in series to DC voltage so that the fundamental component of the voltages, cancelled. This helps in reducing the insulation of the equipment and achieving a better level in control characteristics [11-14].

To obtain control of the magnetic saturation for MCRs, not only the winding connection but also the magnetization characteristics is important. When the DC control excitation current is zero, the working windings inductance is at a maximum, and the current in the winding is at a minimum. In this case, the MCR is equivalent to the transformer no-load operation.

Manuscript published on 30 September 2019
* Correspondence Author
Samuel Addo Darko*, School of Automation and Electrical Engineering, Lanzhou Jiaotong University, Lanzhou 730070, China. (addodarko2@yahoo.com)
Mingxing Tian, School of Automation and Electrical Engineering, Lanzhou Jiaotong University, Lanzhou 730070, China. (tianmingxing@mail.lzjtu.cn)
Huiying Zhang, School of Automation and Electrical Engineering, Lanzhou Jiaotong University, Lanzhou 730070, China. (zhanghylz@163.com)

However, when the DC control excitation current is introduced and gradually increased, the working windings current also increases. This implies that when the control current (excitation) changes, the magnetic saturation level of the iron core also changes. Therefore, the magnetic permeability of the core alters and the impedance value of the MCR is adjusted accurately according to the formula:

$$X = \omega L = \omega \frac{\mu N_{\mathrm{A}}^{2} S_{\mathrm{c}}}{l_{\mathrm{c}}} \qquad (1)$$

Where $\omega = 2\pi f$ is angular frequency, S_c is cross sectional area of the core, l_c is effective length of the magnetic circuit, μ is magnetic permeability, and N_A is winding turns. The magnetization curves are shown in Fig.3(a) and Fig.3(b). The *ab* segment is a linear region and the *bc* segment is a saturation region where the relative magnetic permeability μ is gradually reduced, and it is, therefore, convenient for the inductance adjustment.

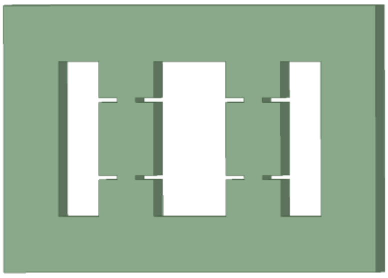

(a) Core structure

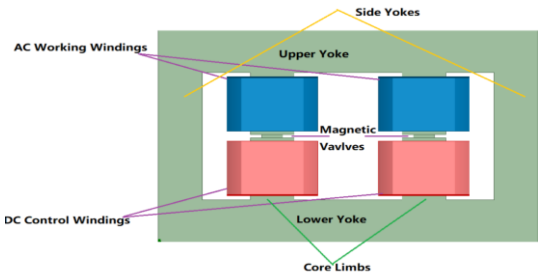

(b) Winding arrangement

Fig.1. structure of MCR

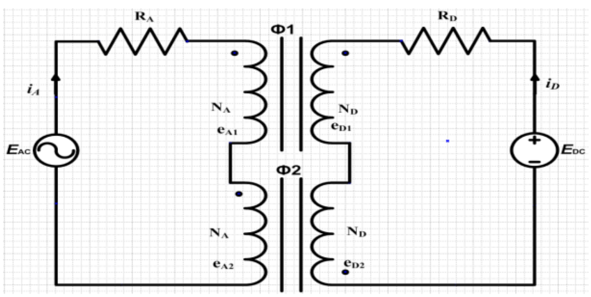

(a) Equivalent circuit

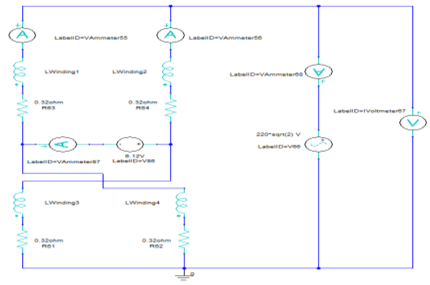

(b) Simulation circuit

Fig.2. circuit of MCR

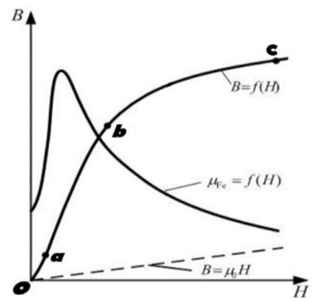

(a) Magnetization curves and permeability curve

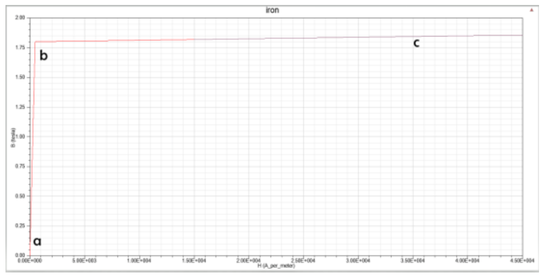

(b) Simulation B-H magnetization curve

Fig.3. Magnetization performance of a core

The average magnetic path length of the MCR is l, the magnetic flux and the magnetic field strength of the core 1 and core 2 are Φ_1, Φ_2, H_1, H_2, combined with the structure of the MCR and the equivalent circuit, its basic equation can be expressed as follows:

$$\begin{cases} E_{\mathrm{AC}} = E_{\mathrm{m}} \sin \omega t = i_{\mathrm{A}} R_{\mathrm{A}} + N_{\mathrm{A}} \left(\dfrac{d\phi_1}{dt} + \dfrac{d\phi_2}{dt} \right) \\ E_{\mathrm{DC}} = i_{\mathrm{D}} R_{\mathrm{D}} + N_{\mathrm{D}} \left(\dfrac{d\phi_1}{dt} - \dfrac{d\phi_2}{dt} \right) \\ lH_1 = i_{\mathrm{A}} N_{\mathrm{A}} + i_{\mathrm{D}} N_{\mathrm{D}} \\ lH_2 = i_{\mathrm{A}} N_{\mathrm{D}} - i_{\mathrm{D}} N_{\mathrm{D}} \end{cases} \qquad (2)$$

Moreover, the relationship between magnetic flux and flux density is: $\Phi = B \cdot S_c$. Since the core structure and the winding arrangement of the reactor are both symmetrical structures, the magnetic flux density has the following relationship:

$$\begin{cases} B_1(\omega t) = -B_2(\omega t + \pi) \\ B_2(\omega t) = -B_1(\omega t + \pi) \end{cases} \qquad (3)$$

Under a normal working condition, the magnetic flux density is generally a non-sinusoidal wave.

$$B_1(\omega t) = B_D + B_{1m}\sin(\omega t + \varphi_1) + B_{2m}\sin(2\omega t + \varphi_2) + B_{3m}\sin(3\omega t + \varphi_3) + \cdots \tag{4}$$

$$B_2(\omega t) = -B_D + B_{1m}\sin(\omega t + \varphi_1) - B_{2m}\sin(2\omega t + \varphi_2) + B_{3m}\sin(3\omega t + \varphi_3) - \cdots \tag{5}$$

The induced voltage of the working winding can be derived as:

$$e_A = e_{A1} + e_{A2} = \omega N_A S_c \left(\frac{dB_1}{dt} + \frac{dB_2}{dt}\right) \tag{6}$$

$$e_A = 2\omega N_A S_c \left[B_{1m}\cos(\omega t + \varphi_1) + B_{3m}\cos(3\omega t + \varphi_3) + \cdots\right] \tag{7}$$

It can be seen from (7) that the MCR working current i_A does not contain even-order harmonics but only contains odd-order harmonics.

III. SIMULATION MODEL OF MCR

A single phase magnetic-valve controllable reactor prototype used to carry out this experiment has the following circuit parameters: N_T=200, N_D=6, B_s=1.8T, R_T=0.32Ω, E_{AC}=220V/50Hz, E_{DC}=6.12V. Moreover, the structural parameters are shown in Tab.1. A three-dimensional model is built by ANSYS and the method of transient analysis was applied in the simulation because it simultaneously has both AC and DC voltages. The magnetic field distribution, the range of the inductance adjustments and output waveform of the working current are mainly analyzed with control voltages of 0V, 0.3V, 2V, 3.06V, 4V and 6.12V.

Tab.1. Structural Parameters of MCR

Main Core (mm^3)	Side Yoke (mm^2)	Core Limb (mm^2)	Magnetic Valve (mm^2)
440×65×310	65×65	65×65	21.7×65

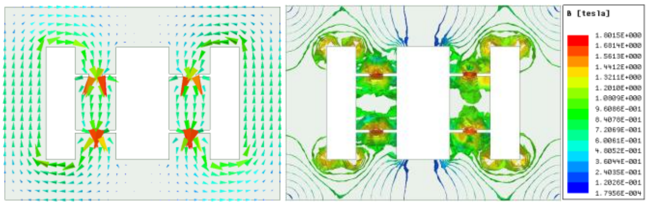

(a) Magnetic flux direction (b) Magnetic flux density

Fig.4 Magnetic flux distribution of MCR in a cycle at *t* = 9.99s

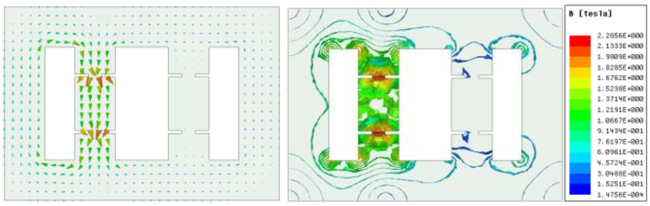

(a) Magnetic flux direction (b) Magnetic flux density

Fig.5 Magnetic flux distribution of MCR in a cycle at *t* = 3.01s

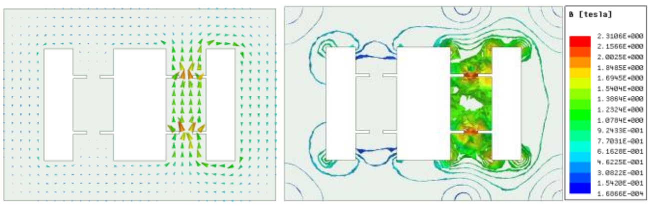

(a) Magnetic flux direction (b) Magnetic flux density

Fig.6 Magnetic flux distribution of MCR in a cycle at *t* = 3.02s

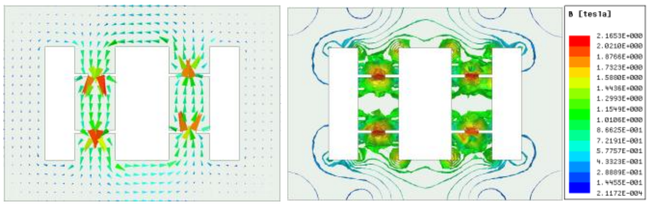

(a) Magnetic flux direction (b) Magnetic flux density

Fig.7 Magnetic flux distribution of MCR in a cycle at *t* = 0.515s

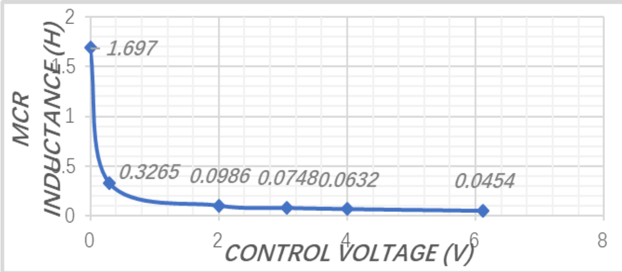

Fig.8 MCR inductance curve

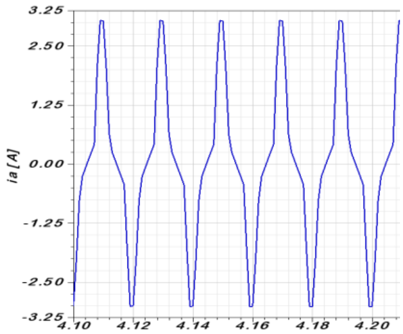

(a) Steady state I_{AC}=3.0336A at E_{DC}=0.3V

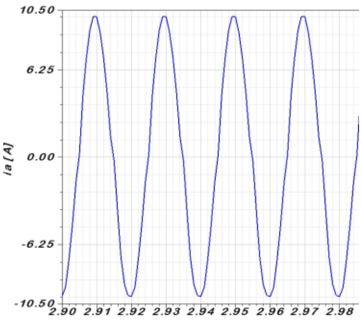

(b) Steady state I_{AC}=10.0390A at E_{DC}=2V

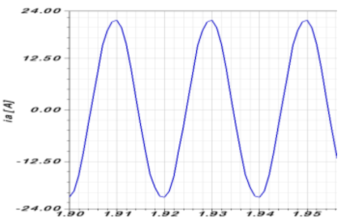

(c) Steady state I_{AC}=21.2343 at E_{DC}=6.12V

Fig.9. Simulation waveforms of working current

IV. ANALYSIS

The magnetic flux distribution inside the core in one cycle during the steady state under different operating conditions is shown in Fig.4 to Fig.7. It can be seen that magnetic flux in the side yokes is uniformly distributed whereas magnetic flux in the core limbs is unevenly distributed due to the magnetic valves in them. However, in this special although common case, the magnetic valves caused the MCR to operate in the *bc* section of the saturation region.

It can be seen from Figs.4(a) and (b) that the magnetic flux is mostly concentrated in-between side yokes and core limbs, leaving middle of upper yoke and lower yoke with least flux. In this instance, there is no DC current in the control winding, and the core limbs have mainly the AC flux generated by the working winding. Therefore, most of the AC flux flow through the side yokes and core limbs, so the working state of the MCR is equivalent to a no-load transformer, and the reactive value of the working winding is very large with small flow of current. The maximum magnetic flux density is approximately 1.805T.

From Figs.5(a) and (b), it can be seen that when control voltage is set to 2V, at time t=3.01s, the left core limb of the MCR has more magnetic flux, followed by the left-side yoke, the right-side yoke and the right core limb respectively. This is because, at this moment, the AC in working winding of the MCR has a magnetic flux direction in the left and right core limbs, and DC in control winding controls the winding in the direction of the left core limb but produces DC flux opposite to the flux of the working winding in the right core limb. Therefore, the magnetic fluxes of opposite directions acting on the right core limb cause the magnetic flux density to the right core limb to be weakened, and the magnetic fluxes in the left core limb are in the same direction, thereby, enhancing the magnetic flux density. The magnetic flux density maximum value is approximately 2.2865T.

From Figs.6(a) and (b), it can be seen that at time t=3.02s in the second half cycle when control voltage is maintained at 2V, the magnetic flux on the right side of the core limb is denser, followed by the right-side yoke, left-side yoke, and the magnetic flux on the left limb is the least. This is because over time, the working winding current value is reversed and the magnetic flux generated by the working winding on the right core limb goes in the same direction as the magnetic flux generated by the control winding, thereby increasing the magnetization. The working winding generates a magnetic flux on the control winding which causes the left core limb to demagnetize. The maximum magnetic flux density is approximately 2.3106T.

When control voltage is set to the maximum rated value (6.12V), it can be seen from figs.7(a) and (b) that at time t=0.515s, most of the magnetic flux are circulating between the left and right core limbs. In this case, over some period of time, the working winding current is zero, and the core limbs have mainly the DC flux generated by the control winding. Therefore, most of the DC flux flow through the left and right core limbs, and a small amount of DC flux passes through the left-side yoke and right-side yoke, which is consistent with the basic principles of MCR.

The impedance of the MCR is $Z = E_{AC}/I_{AC}$. According to the given data and simulation results, X_L is far greater than R_T, therefore, Z is used as X_L. The relationship between reactance and inductance is $X_L = \omega L = 2\pi fL$. The control voltage is adjusted in the range 0V to 6.12V and the change of inductance value can be obtained as shown in Fig.8. It can be seen from the figure that the equivalent AC inductance value of the working winding can be smoothly varied with the change of the control excitation.

The operating current of the MCR is also analyzed based on the above working principle and equations. The waveforms shown in Fig.9 are simulation waveforms of the AC working current. It can be seen that steady state period in Fig.9(a) is the longest, followed by Fig.9(b) and Fig.9(c) respectively. In addition, the harmonic content in Fig.9(a) is the largest, followed by Fig.9(b) and Fig.9(c) respectively. This implies that time for AC working current to reach steady state and harmonics in MCR vary in proportion to the control excitation. After harmonic decomposition, the 3rd harmonic content is the largest, followed by 5th, 7th, and other odd harmonics, which are all very small. In case of a three-phase MCR, different connections can be used to cancel the 3rd harmonic without taking any other measures. However, filters can be installed for improvement.

V. CONCLUSION

A magnetic-valve controllable reactor worked in the saturation region of the magnetization curve under the joint action of AC and DC excitations. The magnetic flux density at magnetic valves was comparatively the largest of all magnetic field distributions, and the magnetic valves of the left core and the right core were alternatively saturated in one cycle. Therefore, the MCR could adjust the inductance as well as the reactive power output smoothly over a wide range while the DC voltage was changed. In addition, the working output current contained little odd-order harmonics that could be mitigated if filtering device is used or magnetic valves are designed carefully. This research has provided a reliable basis for the performance design of a magnetic-valve controllable reactor.

ACKNOWLEDGMENT

This work was supported by the National Natural Science Foundation of China under Grant 51367010 and Grant 51867012, by the Science and Technology Program of Gansu Province under Grant 17JR5RA083, by the Key R&D Program of Gansu Province under Grant 18 YF1FA058, and by the Program for Excellent Team of Scientific Research in Lanzhou Jiaotong University under Grant 201701.

REFERENCES

1. Shi, Peng Tai, M. X. Tian, and Y. N. Guo. "Research on the improvement of the quickness and its simulation for magnetic-valve controllable reactor" [C]. 2015 IEEE International Conference on Applied Superconductivity and Electromagnetic Devices (ASEMD) IEEE, 2015.

2. Wang Ziqiang, Yin Zhongdong. "Study on magnetic circuit structure of magnetic valve controllable reactor based on ANSYS" [C]. International Conference on Energy and Environment Technology, pp.59-62, 2009.
3. Pengning Zhang, Lin Li. "Vibration Properties of Two-Stage Magnetic-valve Controllable Reactor" [J]. IEEE transactions on magnetics, vol. 54, no.3, pp. 1-4, 2018.
4. Feshin A, Chudny V S, Belyaev A N. "Transient stability of oil-field isolated power systems with magnetically controlled shunt reactors" [C]. IEEE Nw Russia Young Researchers in Electrical & Electronic Engineering Conference. IEEE, 2016.
5. Wang Ziqiang, Yin Zhongdong. "Study on magnetic circuit structure of magnetic valve controllable reactor based on ANSYS" [C]. International Conference on Energy and Environment Technology, pp.59-62, 2009.
6. Wang Zhiqiang, Yin Zhongdong, Zhou Lixia, et al. "Study on controllable reactor magnetic structure and loss based on ANSYS" [C]. In the 4th IEEE Conference on Industrial Electronics and Application, pp.201-205, 2009.
7. Wenye Liu, Longfu Luo, Shuda Dong, Yunge Lou. "Overview of Power Controllable Reactor Technology" [J]. ELSEVIER Energy Procedia, vol. 17, Pt. A, pp. 483-491, 2012.
8. Boris V. Oleksyuk, Vladimir N. Tulsky, Stefan Palis. "Magnetically controlled shunt reactors as sources of current and voltage harmonics" [J]. IEEE transactions on power delivery, vol. 33, no 4, pp. 1818-1824, 2018.
9. Torbjorn Wass, Sven Hornfieldt, Stefan Valdemarsson. "Magnetic Circuit for a Controllable Reactor" [J]. IEEE transactions on magnetics, vol. 42, no.9, pp. 2196-2200, 2006.
10. Ziqiang W , Zhongdong Y , Po Y , et al. "The finite elements analysis on magnetic field of controllable saturated reactor" [C]. International Conference on Power Electronics & Drive Systems. IEEE, pp. 364-368, 2009.Yang P, Yin Z D, Cui R C, et al. "Analysis of Reactor Magnetic Circuit Based on ANSYS Command Flow" [J]. Advanced Materials Research, 383-390:2256-2261, 2011.
11. Dimitrovski, A., Z. Li, and B. Ozpineci. "Applications of saturable-core reactors (SCR) in power systems" [C]. T&d Conference & Exposition IEEE, 2014.
12. Tümay M, Demirdelen T, Bal S, et al. "A review of magnetically controlled shunt reactor for power quality improvement with renewable energy applications" [J]. Renewable & Sustainable Energy Reviews, 77:215-228, 2017.
13. Tian Mingxing. "Basic theoretical research on controllable reactors of transformer type" [D]. Xi'an：Xi'an Jiaotong University, 2005.
14. Tian Mingxing, YuanDongsheng, An Xiao, et al. "Analysis on Winding Current of Controllable Reactor of Transformer Type" [J]. High Voltage Engineering, vol. 40, no. 1, pp. 269-274, 2014.
15. Chen B, Kokernak J M. "Thyristor controlled two-stage magnetic-valve reactor for dynamic VAr-compensation in electric railway power supply systems"[C]. IEEE Applied Power Electronics Conference & Exposition, 2000.
16. Tian M, Jin L, Shi P, et al. "A Novel Quickness Improvement Method of a Magnetic-valve Controllable Reactor" [J]. IEEE Transactions on Applied Superconductivity, 26(7), 1-5, 2016.
17. Baodong B , Zhiwei C , Dezhi C. "Design and study on control system of new controllable reactor based on two-phase magnetic material" [C]. Intelligent Control & Automation. IEEE, 2015.
18. B. I. Bazylev, M. A. Bryantsev, S. V. Dyagileva, A. I. Lur'ye, A. A. Negryshev, et al. "A Source of Reactive Power at A 35-Kv Substation of the Vankor Oilfield" [J]. Russian electrical engineering, vol. 83, no. 3, pp. 176-178, 2012.
19. Bryantsev A , Bryantsev M , Bazylev B , et al. "Power compensators based on magnetically controlled shunt reactors in electric networks with a voltage between 110 kV and 500 kV" [C]. IEEE/PES Transmission & Distribution Conference & Exposition, Latin America. IEEE, pp. 239-244, 2011.
20. Weining W , Kai H , Di W , et al. "Study and analysis of magnetic flux controlling continuously adjustable reactor" [C]. China International Conference on Electricity Distribution. IEEE, cp0299, pp. 1-5, 2016.
21. Ji H W, Wen Y Q. "Magnetic Field Analysis of MSMA Actuator Based on ANSYS" [C]. International Symposium on Computational Intelligence & Design. IEEE, 2011.

AUTHORS PROFILE

Samuel Addo Darko, is currently an M.Sc. student at the School of Automation and Electrical Engineering, Lanzhou Jiaotong University, China. He received the B.Sc. degree in Electrical and Electronic Engineering from Kwame Nkrumah University of Science and Technology, Ghana in 2015. He received Higher National Diploma in Electrical and Electronic Engineering from Kumasi Polytechnic, Ghana in 2010. His research interests include electrical machines and applications, hybrid compensation system and its power theory in power system.

Mingxing Tian, is a Professor with the School of Automation and Electrical Engineering, Lanzhou Jiaotong University, China. He is the Director of the Electric Automation Engineering Laboratory of Rail Transit in Gansu Province. He received the B.Sc. degree from Northern Jiaotong University in 1990, and the M.Sc. degree from Southwest Jiaotong University in 1994, and the Ph.D. degree from Xi'an Jiaotong University in 2005. Dr. Tian was a Senior Visiting Scholar at University of Osaka, Japan and University of California, San Diego, 2007 and 2014 respectively. He has supervised over 30 scientific research projects and published nearly 200 academic papers. He is mainly engaged in the research of power quality analysis and control, motor design and control system, power electronics technology and its applications.

Huiying Zhang is a Ph.D. student at the School of Automation and Electrical Engineering, Lanzhou Jiaotong University, China. She received the M.Sc. degree from Henan Polytechnic University, China in 2008. She also received the B.Sc. degree from Henan Polytechnic University, China, in 2003. Her main research area is calculation and analysis of the characteristics of magnetically saturated controllable reactor.